JOURNAL OF GEOPHYSICAL RESEARCH, VOL. 106, NO. A9, PAGES 18,969–18,979, SEPTEMBER 1, 2001

Polar observations of topside field-aligned O^+ flows and auroral forms

B. A. Stevenson,[1,2] J. L. Horwitz,[1] G. Germany,[1] T. E. Moore,[3] B. L. Giles,[3] P. D. Craven,[4] M. O. Chandler,[4] Y.–J. Su,[5] and G. K. Parks[6]

Abstract. Measurements of thermal O^+ ion densities, field-aligned velocities, and fluxes from the Thermal Ion Dynamics Experiment (TIDE) on Polar obtained near 5000 km altitude over the Southern Hemisphere are compared with auroral images from the Ultraviolet Imager (UVI). Three passes were selected for analysis in this paper based on data availability from the TIDE and UVI instruments. Results indicate upward O^+ flows in the cleft region but downward O^+ flows in the polar cap region. Also, the O^+ ion density follows a decreasing trend from the poleward side of the cusp region into the nightside aurora region. The magnitude of the downward O^+ parallel velocities increases from dayside to nightside across the polar cap boundary. The upflows tend to occur over or near auroral forms, while the downflows are seen in relatively dark regions, such as the polar cap. These results are consistent with a cleft ion fountain source for the polar cap O^+ ions. In the nightside polar cap, the results indicate a transition from downward to upflowing field-aligned O^+ ions near boundaries of bright auroral arcs.

1. Introduction

The ionosphere has been shown to be a principal source of magnetospheric plasma [*Horwitz*, 1982, 1987, 1995; *Shelley et al.*, 1982; *Moore et al.*, 1986; *Chappell et al.*, 1987; *Moore and Delcourt*, 1995; *Ganguli*, 1996; *Horwitz and Moore*, 1997; *Andre and Yau*, 1997; *Yau and Andre*, 1997; *Knudsen et al.*, 1998; *Abe et al.*, 1993, 1998; *Miyake et al.*, 1993, 1996; *Norquist et al.*, 1998; *Shelley*, 1995; *Yau et al.*, 1985]. *Lockwood et al.* [1985a] showed that high fluxes of upward field-aligned suprathermal O^+ are found near the dayside polar cap boundary, or cleft region. The upward flows near the dayside polar cap boundary act as a source of heavy ions (O^+) for the polar cap region of the magnetosphere [*Lockwood et al.*, 1985a]. *Horwitz and Lockwood* [1985] used a kinetic model to investigate various aspects of the cleft ion fountain (CIF).

The CIF model considered the upwelling ions in the cusp region and how they are influenced by parallel electric fields, $\mathbf{E} \times \mathbf{B}$ convection drift across the polar cap, and gravitational forces. The model illustrated that for heavy ion species such as O^+, the high-energy ions would maintain upward flow velocities at high altitudes throughout the polar region [*Horwitz and Lockwood*, 1985]. *Su et al.*, [1998b] presented Polar/Thermal Ion Dynamics Experiment (TIDE) data showing upward O^+ flow at 8 Earth radii (R_E) throughout the polar region. However, the CIF model also illustrated that the lowest-energy ions, including O^+, would follow a parabolic trajectory, resulting in downward O^+ in the polar cap region, as was reported in the high-latitude polar cap at 5000 km by *Su et al.*, [1998b]. In contour plots of parallel fluxes, *Horwitz and Lockwood* [1985] indicated that there is a demarcation line between downward flows (below) and upward flows (above). This demarcation line should generally rise from low altitudes of 2000–4000 km near the cleft region to a few R_E moving antisunward into the nightside polar cap, depending chiefly on the convection speed and cleft ion energization [*Horwitz and Lockwood*, 1985]. Furthermore, for low-energy ions with a large initial pitch angle, the magnetic gradient force can dominate over the gravitational force, resulting in "hopping" trajectories [*Horwitz and Lockwood*, 1985].

Pollock et al. [1990] showed that O^+ was the dominant upwelling ion species below 3 R_E in the dayside cleft region. O^+ velocity observations by DE 1 displayed upflows in the dayside cusp region and aurora latitudes while showing downflows in the polar cap regions [*Chandler*, 1995].

Both discrete and diffuse aurora are considered sources of ionospheric ions for the magnetosphere. The high-latitude topside ionosphere and lower magnetosphere involves several ion acceleration processes including auroral parallel potential drops, wave-particle interactions, and ambipolar electric fields [e.g., *Hultqvist et al.*, 1988; *Chang et al.*, 1986; *Andre' et al.*, 1990; *Crew et al.*, 1990; *Hultqvist*, 1996; *Banks and Holzer*, 1968; *Nagai et al.*, 1984; *Lockwood et al.*, 1985b; *Chandler et al.*, 1991; *Abe et al.*, 1998]. Various mechanisms that energize ionospheric ions along geomagnetic field lines have been modeled using moment-based simulations [e.g., *Schunk and Sojka*, 1997], and semikinetic [e.g., *Wilson*, 1992] and coupled fluid-semikinetic models [e.g., *Su et al.*, 1998a; *Estep et al.*, 1998; *Wu et al.*, 1999].

In terms of links with observed auroral forms, *Hirahara et al.*, [1998] presented observations at 5000 km altitude showing upflowing ionospheric ions in and near auroral forms. Low-energy upflowing conic distributions were observed at slightly higher latitudes than the discrete aurora,

[1]Center for Space Plasma and Aeronomic Research, University of Alabama in Huntsville.
[2]Now at Axcelis Technologies, Beverly Massachusetts.
[3]Laboratory for Extraterrestrial Physics, Goddard Space Flight Center, Greenbelt, Maryland.
[4]Space Sciences Laboratory, Marshall Space Flight Center, MSFC, Alabama.
[5]Space and Atmospheric Sciences, Los Alamos National Laboratory, Los Alamos, New Mexico.
[6]Geophysics Program, University of Washington, Seattle, Washington.

Paper number 2000JA003042
0148–0227/01/2000JA003042$09.00

while higher-energy upflowing beam distributions were observed over discrete aurora [*Hirahara et al.* ,1998].

The Polar spacecraft was launched into an elliptical Earth orbit in February 1996 at a 90° inclination, with a 9 R_E geocentric distance at apogee and a 1.8 R_E geocentric distance at perigee. Several instruments onboard Polar measure plasma properties, observe auroras, and measure electric and magnetic fields and waves. The TIDE [*Moore et al.*, 1995] instrument provides high resolution, mass resolved in situ measurements of core ions (0.3–450 eV) in both the high- and low-altitude polar magnetosphere. The ultraviolet imager (UVI) instrument provides 36 s images which give information, such as intensity, structure, and position of aurora phenomena [*Torr et al.*, 1995].

TIDE has demonstrated O^+ ionospheric outflows into the magnetosphere in the cleft regions [e.g., *Su et al.*, 1998b], which are consistent with earlier DE 1 observations presented, for example, by *Lockwood et al.*, [1985b]. *Su et al.*, [1998b] analyzed Polar TIDE ion observations and found field-aligned downward O^+ in the polar cap region. They also reported that the density of O^+ decreases from the dayside to the nightside polar region in direct relationship to the increase in solar zenith angle [*Su et al.*, 1998b].

Su et al., [1998b] only examined TIDE ion observations for the isolated polar cap region above 80° invariant latitude. It is important to extend the analysis to include the auroral and cleft regions in order to understand the complete ion transport from source region into regions of no energization. In a previous study using TIDE and UVI observations, *Hirahara et al.*, [1998] presented "chromograms" indicating features of ions at 5000 km with companion auroral images. However, to our knowledge, there has been no previous study of observations of topside/lower magnetosphere thermal ionospheric ion flows characterized in terms of O^+ density, flow velocity, and flux being compared with near-simultaneous auroral images. In this paper we present the first such comparison of these ionospheric ion up/down flows and optical auroral emissions for the high-latitude ionosphere.

2. Data Analysis

In this paper we will present TIDE O^+ moment data and UVI auroral observations for three Polar perigee passes (~5000 km), in April and May of 1996. TIDE measures three-dimensional ion distribution functions in the 0.3–450 eV energy range with a 6 s time resolution, corresponding to the Polar spin period [*Moore et al.*, 1995]. In this analysis, however, to statistically improve the trends seen, the data have been averaged over five spins, resulting in 30 s intervals. Density, three-dimensional bulk velocities, and parallel and perpendicular temperature moments are obtained for the thermal ion portion of these measured distribution functions according to the analysis of *Su et al.*, [1998b]. The analysis techniques include an iterative "filling-in" procedure used to estimate and include the contribution of ions screened by the normally positive spacecraft potential [*Su et al.*, 1998b]. The resulting velocity, density, and flux data allow in-depth analysis of the processes that are occurring in the transition region between the polar cap and the auroral oval. The TIDE instrument also detects H^+ and He^+ [e.g., *Su et al.*, 1998b]. However, in this paper we focus only on the O^+ for comparison with the UVI auroral measurements. As discussed, for example, by *Horwitz and Moore* [1997], the O^+ within the normal polar cap is expected to be convected from a CIF or auroral source, while the polar cap H^+ is mostly from a more locally produced polar wind source. It is also believed that generally, the light ion densities are minor species at these altitudes from both observational [e.g., *Su et al.*, 1998b] and simulation [e.g., *Wu et al.*, 1999] bases. Also, because of the smaller "ram" energy of the light ions, much of their velocity distribution is not observed owing to the positive spacecraft charging at these altitudes, and analysis for bulk parameters is generally more difficult than for the O^+ distributions. It is even possible that derived light ion densities are lower than the actual densities present if too much of the distribution is shielded. Therefore we have focused only on the O^+ parameters for comparison with the auroral measurements in this paper.

The B_z component of the interplanetary magnetic field (IMF) is southward for each of the three cases presented within this paper. The southward IMF should result in antisunward convection across the polar cap. Several Polar perigee passes were also examined during which the IMF was northward (for example, on April 29, 1996). However, we found on those passes that the density was frequently below the detection threshold. Also, we expect that during such northward IMF periods, the convection should be more complex. This may include regions of Sun-aligned arcs involving sunward convection, which is different from the CIF picture for O^+ parallel flows during the nominal two-celled convection generally observed during southward IMF conditions. The nightside aurora does not provide a large source of upflowing ions like the cusp region does, leaving the polar cap with much lower ion densities. Some passes were observed with near-zero B_z components that fluctuated between positive and negative. During these periods, ions were often still detected within the polar cap, most likely due to the periods of southward IMF.

The UVI instrument observes auroral emissions with wavelengths ranging from 130–170 nm. UVI uses a set of five filters, three mirrors, and a charge-coupled device (CCD) system to produce images of auroral excitation with a time resolution of 36 s [*Torr et al.*, 1995]. UVI cannot detect UV emissions with intensities below 100 R. UVI has a field of view and angular resolution of 8° and 0.04°, respectively. During perigee (~5000 km), the area observed is ~980 × 963 km^2. Fine structure in the aurora can be seen due to a higher spatial resolution (~4.9 × 4.3 km^2) despite the well-defined wobble seen in UVI perigee data.

Another benefit of using UVI is that the ultraviolet wavelength range makes it possible to view dayside auroral arcs despite background dayglow emissions. Besides the instrument background, the dayglow was also subtracted from the auroral emissions in regions of solar illumination. The dayglow emissions did not change significantly across the ~980 × 963 km^2 viewing area, which allowed a local average dayglow value to be subtracted from the images.

A minor cautionary note is in order regarding the timing of the UVI images presented and the TIDE parallel O^+ flows. The TIDE measurements, of course, are direct in situ ion measurements. These measurements pertain directly to the spatial location in terms of invariant latitude, etc., during the indicated universal times (UT), for flows at the 5000 km altitude of the Polar spacecraft. The UVI measurements, however, are remote observations of the auroral emissions from the lower ionosphere, generally 120–200 km altitude. Also, the UVI viewing direction was varied, particularly during

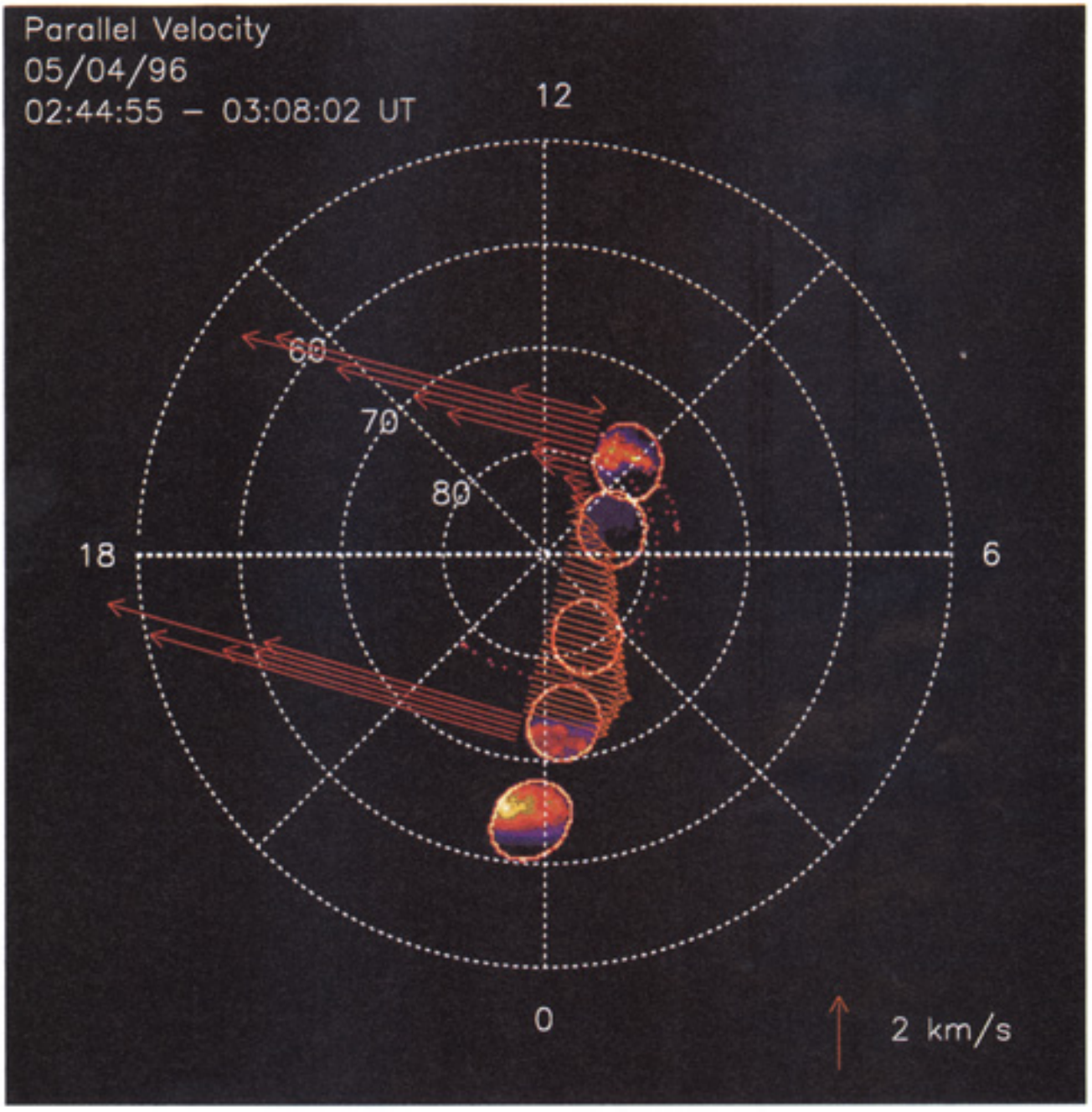

Plate 1. Ultraviolet Imager (UVI) images superimposed on the O^+ parallel velocity as a function of spacecraft position on May 4, 1996, for 0245–0308 UT. The images demonstrate the position of the dayside and nightside auroral boundaries. The downward parallel velocities are displayed in orange, while the upward parallel velocities are shown in red. The red-dotted partial circular segments are artifacts of the image production process that we have been unable to remove and should be ignored.)

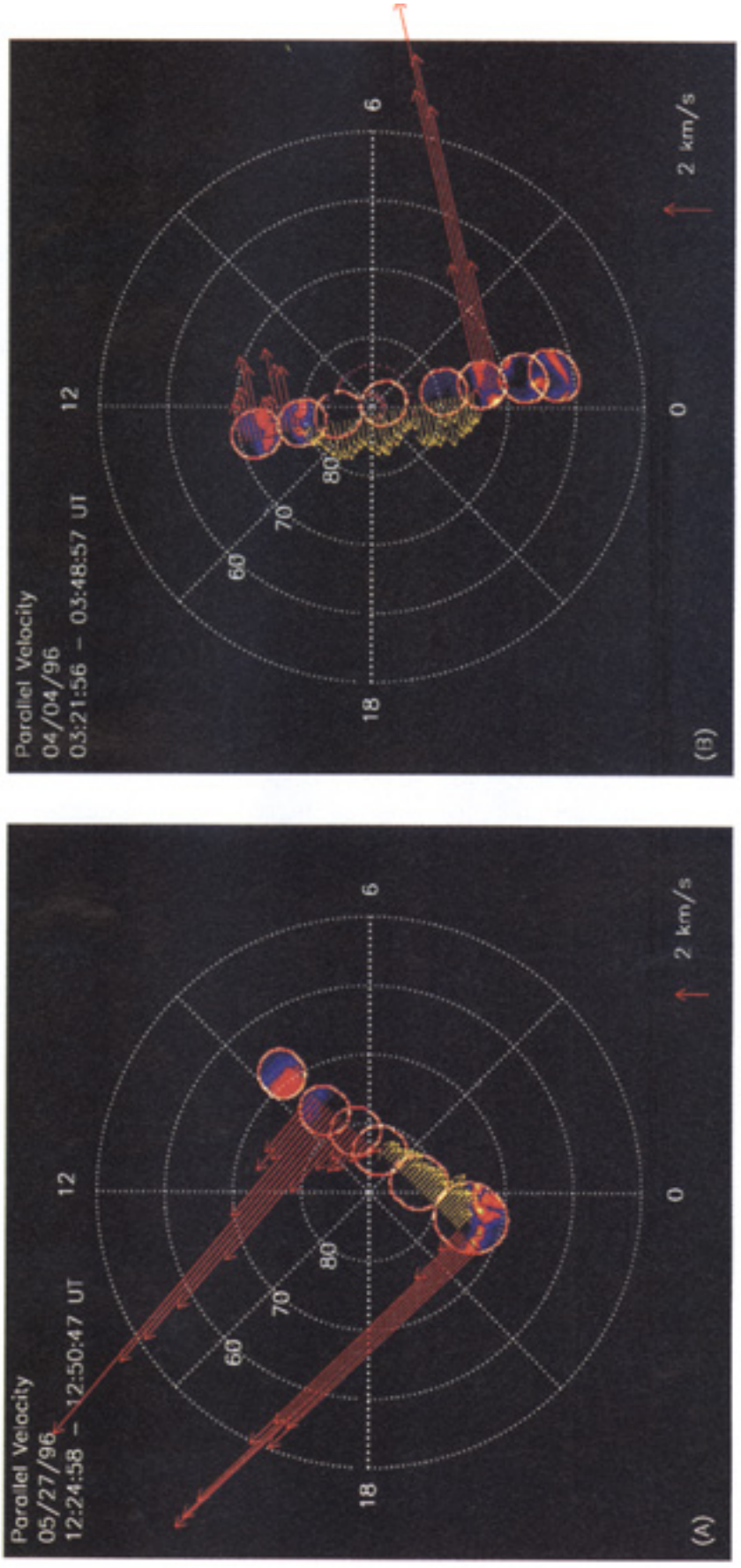

Plate 2. UVI images superimposed on the O^+ parallel velocity as a function of spacecraft position on (a) May 27, 1996, for 1225–1251 UT, and (b) April 4, 1996, for 0322–0349 UT. The downward parallel velocities are displayed in orange, while the upward parallel velocities are shown in red. The red-dotted partial circular segments are artifacts of the image production process that we have been unable to remove and should be ignored.)

perigee passes. The camera may point either somewhat ahead or behind the spacecraft field line on which Polar resided at a given universal time. The net result is that there can be offsets as large as 3 min between when the TIDE measurements were made for a given invariant latitude and the times that UVI measured auroral emissions from that latitude. Transit times between auroral processes causing upflows at lower altitudes and when those ions reach the 5000 km altitude of Polar TIDE (including $\mathbf{E} \times \mathbf{B}$ convection effects) are most likely comparable or even larger than these offsets.

Finally, in order to clearly display UVI images, the border of each UVI image was represented by a light-orange border to identify the UVI viewing area. Because of the substantial differences between dayside and nightside auroral intensities, and other reasons, the absolute auroral intensities were not displayed. In order to clearly present the location and structure of the aurora, the displayed images have been scaled. However, the relative auroral intensities within each image have not been changed. The absolute auroral intensities can be obtained through the UVI Web site at www.ssl.msfc.nasa.gov/uvi/default.htm. Where two UVI images overlap, the more current (later in universal time) image was used in order to correlate with the in situ TIDE data.

To further understand the relationships between the O+ flows and aurora, Figures 1, 2, and 3 display the relative auroral intensities as a function of position. For an ideal comparison, the UVI field of view would be centered on the TIDE footprint. Unfortunately, the UVI field of view is typically not centered on the TIDE footprint and often does not include the footprint. For those cases where the TIDE foot point is not contained within the UVI field of view, a portion of the UVI image closest to the TIDE foot point was selected to be representative of the auroral form sampled by the TIDE data. This approximation is expected to be valid when the UVI field of view is close to the TIDE foot point and the auroral form is not changing rapidly compared with the transit time of the TIDE foot point across the aurora. The data in this paper have been restricted to passes when the TIDE spacecraft track intersects or is adjacent to the UVI field of view. Therefore this approximation should be valid for the data presented in this paper.

In order to compare the TIDE and UVI data, a region of interest (ROI) in invariant latitude and magnetic local time (MLT) was defined about each TIDE foot point. The size of the ROI was set by the relative spacing between each TIDE foot point so that the ROIs did not overlap. The portion of the UVI image that intersected this ROI was averaged to approximate the auroral intensity at the TIDE foot point location. Pixels in the UVI images with no auroral intensity were not included in the averaging process. Because of the high spatial resolution of the UVI images at perigee, the auroral forms largely fill the UVI field of view. Thus, while the averaging process may be inappropriate for higher-altitude images with large amounts of structure, it is appropriate for the data presented here. For situations where multiple UVI images overlapped a given ROI, the latest UVI image was used.

3. Southern Perigee Pass on May 4, 1996: 0245–0308 UT

Plate 1 displays the O^+ parallel velocity on a polar dial plot of invariant latitude and MLT, for the southern perigee pass on May 4, 1996, at 0245–0308 UT. During the perigee passes discussed, the Polar spacecraft moves sunward across the southern polar region. However, discussion is presented of the data antisunward from the presumed cleft source region to the nightside aurora. As discussed in the previous section, the parallel velocities were derived from TIDE moment data. The magnitudes of these parallel velocities are represented by the arrows, red representing upflowing parallel velocities and orange representing downward parallel velocities. Multiple UVI images are also displayed on the dial plot at their spatial locations along the satellite foot point track. Such successive images are important for an understanding of the large-scale nature of the auroral distribution during this interval. The UVI images available during this pass were collected using the Lyman-Birge-Hopfield (LBH) short filter in the auroral regions and the LBH long filter in the polar cap, both with an 18 s exposure time. We examined data (not shown here) from a Los Alamos National Laboratory (LANL) geosynchronous spacecraft. The LANL geosynchronous electron data show an electron injection during this time period that appears to be substorm related. However, no similar injection was seen in the proton data. The *Kp* index during this time was moderate at 3. The B_Z component of the IMF was found by using Wind data that were time-shifted according to the satellite's position in X_{GSM} to be appropriate to time of interaction with the magnetopause. The value during this time was found to be around –2.2 nT.

Plate 1 displays upflowing O^+ in the dayside cleft region reaching a maximum velocity of 10.3 km s^{-1} at 76° invariant latitude and 0306:30 UT. For reference, an O^+ ion traveling upward at 1 km s^{-1} at the Polar altitude (5000 km) would have had a velocity of approximately 6 km s^{-1} at 1000 km neglecting any acceleration between the two altitudes, although such energization is certainly possible in the range 1000–5000 km [e.g., *Andre and Yau*, 1997]. The magnitude of the upflowing velocities decreased with increasing latitude, eventually becoming a downward flow at 84°, 0302 UT. The downward velocities increased antisunward across the polar cap. The downward velocity reached a maximum of 2.8 km s^{-1} at 78° invariant latitude and 0250:30 UT. UVI did not detect any auroral emission in the polar cap region for this pass, and the downward O^+ velocity increased steadily, until approaching the nightside auroral arc displayed.

By 78° on the nightside, the magnitude of the downward velocity began to decrease with decreasing latitude across the boundary between the polar cap and the auroral forms. The parallel velocity changed abruptly once in the region of discrete aurora from 2.4 km s^{-1} downward to 7.5 km s^{-1} upward flowing velocity. This auroral boundary at 74° (0247 UT) was also seen in the fast plasma analyzer (HYDRA) electron data. These upflowing parallel velocities within the auroral region were even larger (up to 12.0 km s^{-1}) than those measured in the cleft region (10.3 km s^{-1}).

Multiple UVI images are displayed to represent the auroral activity. The images displayed on the nightside appear to show the poleward and equatorward boundaries of the auroral oval. The width of this auroral form is relatively large, spanning approximately 10° in invariant latitude. The images seen in the nominal polar cap region are devoid of auroral emissions. Finally, the dayside UVI image displays the apparent poleward boundary of the dayside aurora. The auroral oval during this period has sharper boundaries than in the following passes.

Figure 1 displays the O^+ density and flux parameters, as well

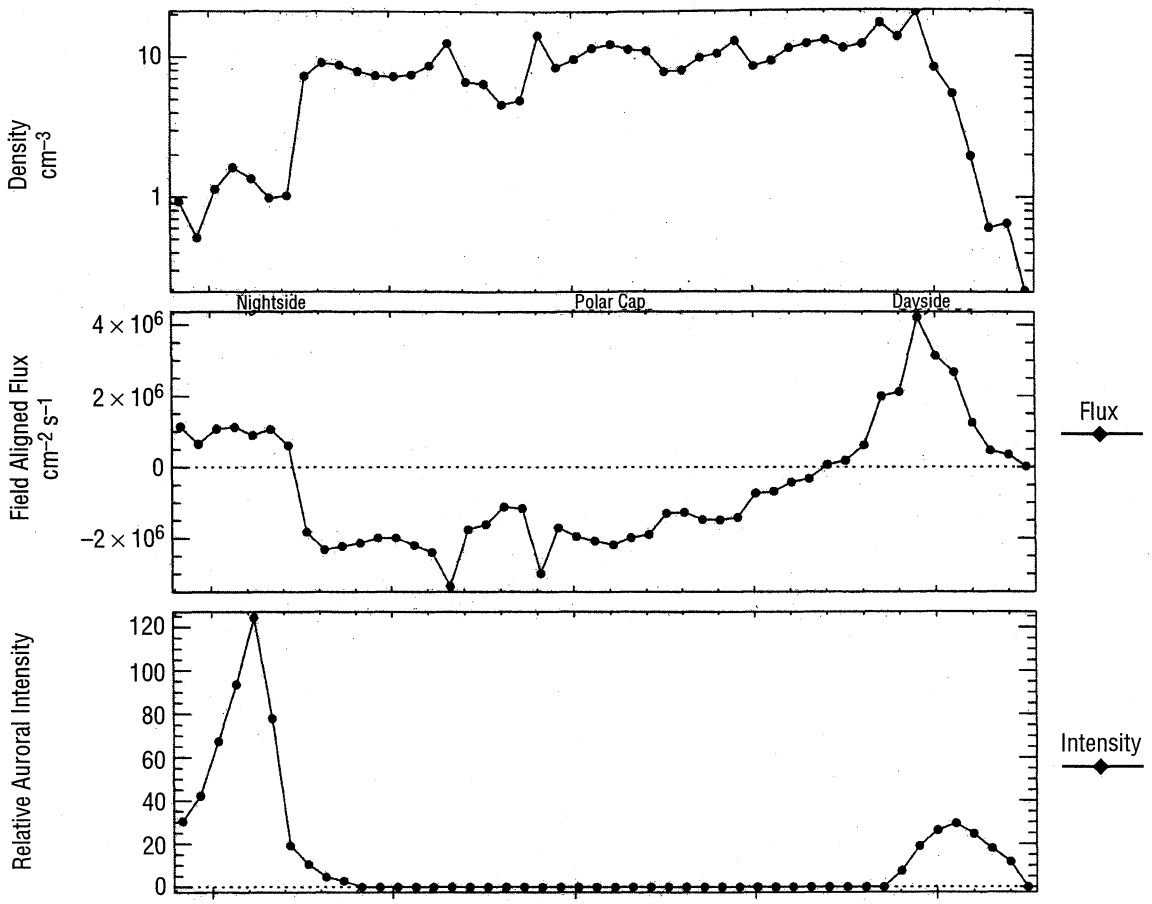

Figure 1. O^+ density and field-aligned flux versus spacecraft position for May 4, 1996, 0245–0308 UT, Polar southern perigee pass. The general day-to-night O^+ density decline is consistent with that of *Su et al.* [1998b].

as relative auroral intensity for this pass with respect to universal time, with the orbital parameters including invariant latitude and MLT of the Polar spacecraft also provided. The plot starts with data for the nightside region corresponding to 0243 UT. The density stayed relatively high throughout the polar region, with a maximum at the poleward side of the cusp region of 20 cm^{-3} at 81° (0304:30 UT). The density appeared to slowly decrease from dayside to nightside (right to left) across the polar cap with a minimum of 0.5 cm^{-3} measured within the middle of the nightside aurora. This antisunward density decline is consistent with the *Su et al.*, [1998b] statistical presentation.

The flux plot in Figure 1 closely follows the trends in the parallel velocities seen in Plate 1, although the density does vary by an order of magnitude. From Plate 1, the poleward boundary of the discrete dayside aurora is seen to be at 80° invariant latitude (0304:30 UT). This dayside auroral boundary is also confirmed in electron data from the HYDRA instrument aboard Polar (also not shown here). The maximum obtained O^+ flux (Figure 1) was that for the cusp region of 4.0×10^6 cm^{-2} s^{-1} at 80° invariant latitude, 0304:30 UT. The flux decreased with increasing latitude, and turned downward at 84° (0302 UT). The magnitude of the downward flux then increased from dayside to nightside, reaching a maximum downward flux of 3.2×10^6 cm^{-2} s^{-1} at 80° on the nightside (0251:30 UT). The flux changed dramatically from 1.7×10^6 cm^{-2} s^{-1} downward to 1.6×10^6 cm^{-2} s^{-1} upward at the boundary of the auroral region at 74° invariant latitude, 0247 UT. The maximum flux observed within the nightside aurora was 1.9×10^6 cm^{-2} s^{-1} at 72°. Finally, the auroral intensity indicates a more intense aurora present in the premidnight sector than in the dayside region.

4. Southern Perigee Pass on May 27, 1996: 1226–1248 UT

Plate 2a displays O^+ field-aligned velocities and UVI images on a polar dial plot, similar to the format of Plate 1, here for the Polar southern perigee pass on May 27, 1996, at 1226–1248 UT. The arrows represent the magnitudes of the parallel velocities, left (red) representing upflowing parallel

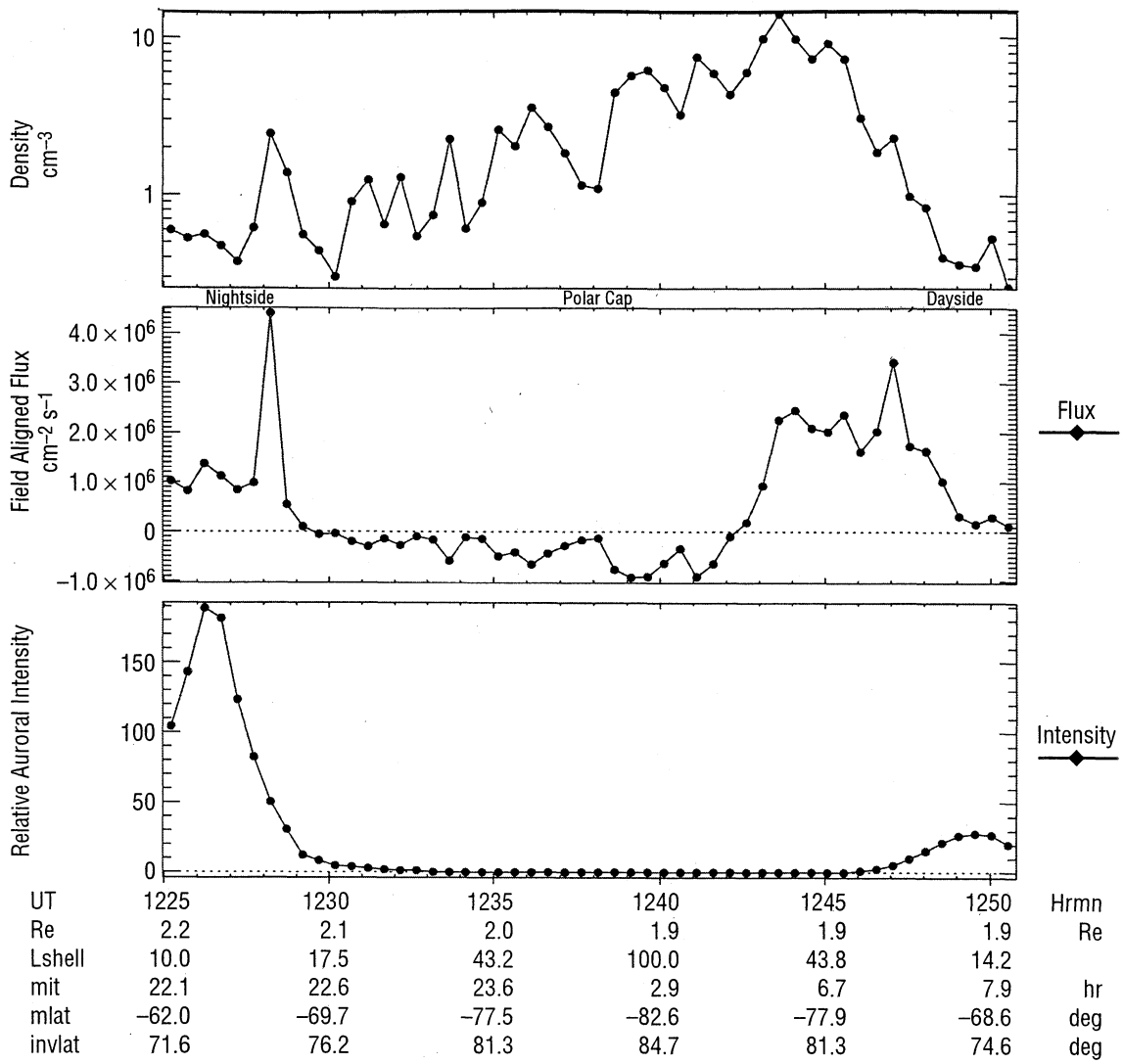

Figure 2. O^+ density, field-aligned flux, and relative auroral intensity as a function of spacecraft position for May 27, 1996, 1225–1251 UT. The general day-to-night O^+ density decline is consistent with that of *Su et al.* [1998b].

velocities and right (orange) representing downward parallel velocities. Multiple UVI images are also displayed on the dial plot centered on their spatial locations as in Plate 1. The UVI images during this pass were collected using LBH long filter and 36 s exposure time. The LANL geosynchronous electron data show an electron injection during this time period that appears to be substorm related. Again, however, the proton data do not show a similar type injection. The IMF B_z component was on average –0.8 nT during this period. The *Kp* index was moderately low at 2–.

Beginning again on the dayside region, the magnitude of the upflowing velocities decreased with increasing latitude toward the polar cap and at 85° (1242 UT) turned downward over the smaller polar cap region. The downward velocity reaches a maximum of 2.6 km s^{-1} at 82° (1233:30 UT). The downward parallel velocities appear to have more structure across the polar cap than in Plate 1.

Multiple UVI images are again displayed along the Polar track to reveal the large-scale auroral distribution. The primary dayside auroral arc was seen between 68° and 76° in invariant latitude. The maximum detected upward velocity in the dayside region was 25.4 km s^{-1}, and occurred just poleward of the dayside aurora, at 77° (1248:30 UT). The nightside aurora appeared between 70° and 75° invariant latitude, and the poleward auroral boundary directly corresponded to the sudden change in parallel velocity from downflows to upflows. The dayside and nightside high-latitude auroral boundaries detected by UVI were again checked against HYDRA electron data (again not shown here) and showed no differences. Within the nightside aurora, the parallel velocity peaked at 73° (1226 UT), with a value of 24.4 km s^{-1}.

Figure 2 displays the O^+ density, flux, and relative auroral intensity with respect to universal time, invariant latitude, and MLT as in Figure 1. The density reached a maximum of 14 cm^{-3} at 83° (1243:30 UT), which is considerably poleward of the dayside aurora. The density then decreased from dayside to nightside across the polar cap until reaching 0.3 cm^{-3} at the nightside auroral boundary. At this boundary (75°), the density increased to 2.5 cm^{-3} but then returned to values of the order of 0.4 cm^{-3} at lower auroral latitudes.

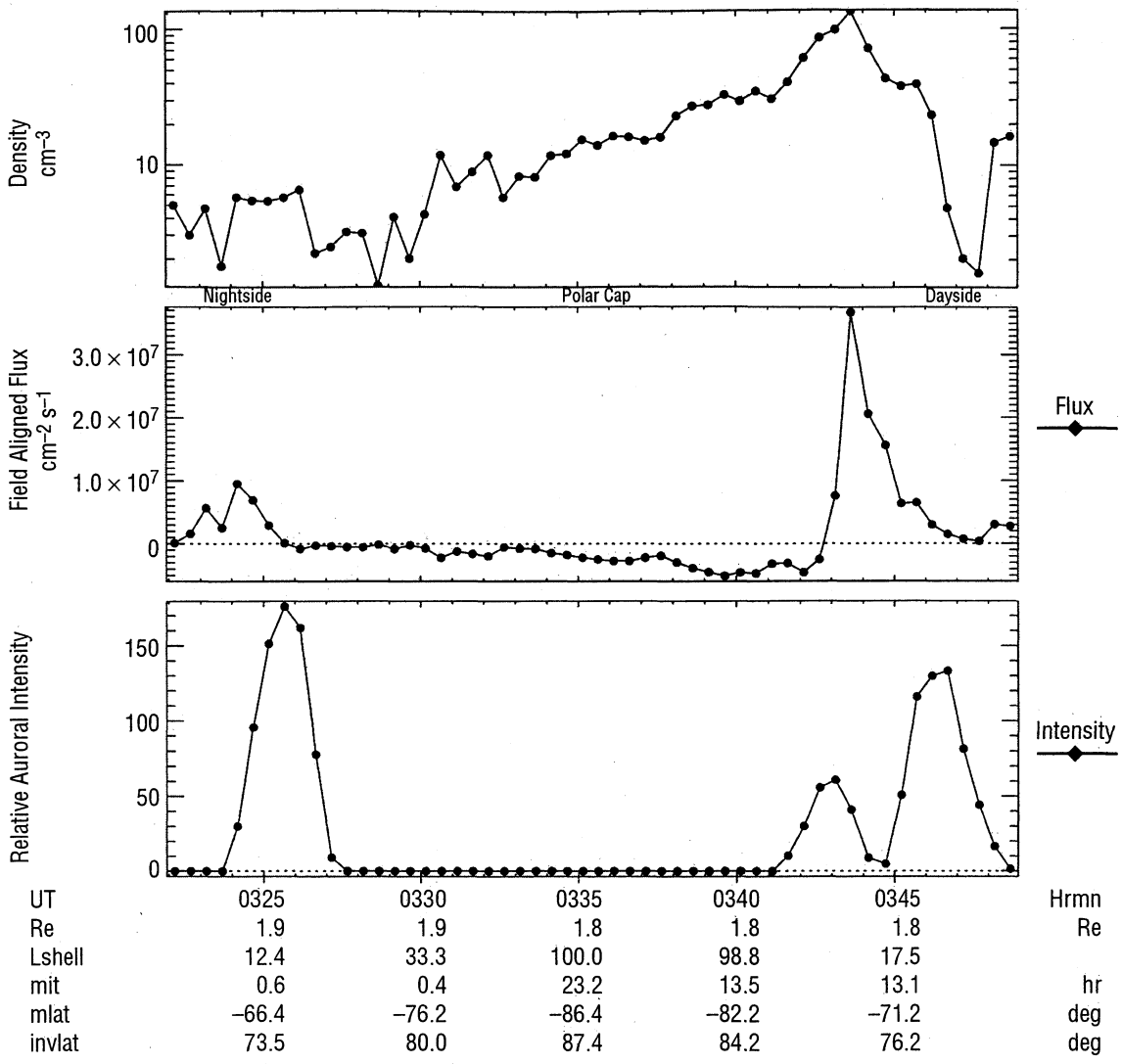

Figure 3. O^+ density, field-aligned flux, and relative auroral intensity as a function of spacecraft position for April 4, 1996, 0322–0349 UT. The general day-to-night O^+ density decline is consistent with that of *Su et al.* [1998b].

The maximum flux of 4.4×10^6 cm^{-2} s^{-1} was at 75° (1228 UT) on the nightside corresponding to the sudden increase in density. The maximum dayside flux was 3.4×10^6 cm^{-2} s^{-1} and occurred at 78° (1247 UT) on the poleward side of the dayside aurora. The magnitude of the downward flux seen in the polar cap region decreases from dayside to nightside. Finally, the auroral intensity again indicates a much more intense aurora present in the premidnight sector than in the dayside region.

5. Southern Perigee Pass on April 4, 1996: 0322–03:49 UT

As in Plates 1 and 2a, Plate 2b displays O^+ field-aligned velocities and UVI images on a polar dial plot, here for the pass on April 4, 1996, at 0322–0349 UT. The magnitudes of the parallel velocities are represented by the arrows, right (red) representing upflowing parallel velocities and left (orange) representing downward parallel velocities. Multiple UVI images are also displayed on the dial plot at their spatial locations as in Plates 1 and 2a. The UVI images were collected using the LBH long filter and 36 s exposure time.

LANL geosynchronous data (not shown) show a substorm-type electron injection around 0000 UT, but only a slight increase in electron flux during this perigee pass. This slight increase may be due only to the thinning of the plasma sheet. Again, no ion injection was seen during this time. The IMF B_z component was again slightly southward, approximately −1.0 nT during this period. The *Kp* index was moderate to low at 2+.

The magnitude of the upflowing velocity within the dayside auroral region between 72° and 82° invariant latitude was low compared with the velocities in Plates 1 and 2a. The maximum velocity in this region was only 3.6 km s^{-1} and varied considerably across the dayside auroral region. The maximum dayside velocity also occurred over the auroral region at 76° (0344:30 UT), rather than poleward of the dayside auroral boundary as in Plates 1 and 2a. The velocity turned downward at the high-latitude dayside auroral boundary and increased in magnitude with increasing latitude until 85° (0339 UT). The magnitude of the downward velocity then decreased with increasing latitude. This oscillating velocity pattern was repeated three times across the apparent polar cap region. At the nightside auroral boundary at 75° (0326 UT), the

downflowing velocity abruptly changed to upflowing. This upward velocity increased with decreasing auroral latitude until reaching a maximum of 16.6 km s^{-1} at 73° (0324 UT). The upward velocity magnitude then decreased in regions of diminished auroral emissions.

The UVI images now show broad auroral regions covering 15° in invariant latitude on the nightside and 10° on the dayside. The auroral emission displayed higher-intensity bands on both the high- and low-latitude boundaries of the aurora, while a decreased intensity was seen in the middle auroral latitudes. As in Plates 1 and 2a, no auroral emissions above the 100 R UVI thresholds were observed within the nominal polar cap.

Figure 3 displays the O^+ density and flux, as well as relative auroral intensity with respect to universal time, invariant latitude, and MLT as in Figure 2. The density reached a maximum of 133 cm^{-3} at 78° (0343:30 UT), which corresponds to the high-latitude boundary of the observed dayside aurora. The density then decreased from dayside to nightside across the polar cap until reaching 1.3 cm^{-3} at the nightside auroral boundary. At this boundary (75°), the density increased to 6.5 cm^{-3} over the region of strong auroral emission.

The maximum flux observed was 3.7×10^7 cm^{-2} s^{-1} at 78° (0343:30 UT), within the dayside aurora. This flux corresponds with the maximum O^+ density. The maximum nightside flux is 9.5×10^6 cm^{-2} s^{-1} and occurs at 73° (0324 UT) within the nightside aurora. The magnitude of the downward flux seen in the polar cap region decreased from the dayside to nightside, as in Figure 2.

The auroral intensity indicates more intense aurora were present in the midnight sector than on the dayside. The intensity plot also shows that the UVI emissions with the dayside aurora are more intense at the high- and low-latitude auroral boundaries. These auroral boundaries were also examined in the HYDRA data and again displayed similar features and boundaries in both the dayside and nightside regions. However, the data were not a direct correlation with the UVI images in the bifurcated dayside auroral region.

6. Summary and Conclusions

The most evident relationship seen within this data set is the relationship between regions of auroral excitation and O^+ upflowing parallel velocities. Upflowing ions at auroral latitudes have been detected in various forms including beam and conic distributions with accompanying auroral images provided [e.g., *Hirahara et al.*, 1998]. However, in this paper we have displayed relationships of O^+ bulk parameters (namely, parallel velocities, densities, and fluxes) to the auroral emissions along the Polar track across the high-latitude ionosphere. We believe these are the first such detailed comparisons of ionospheric ion parallel velocities to auroral emissions presented. As seen in the polar plots of Plates 1, 2a, and 2b, a sharp change in parallel velocity is typically observed at or slightly poleward of the nightside high-latitude auroral boundary. The change in parallel velocity associated with dayside high-latitude auroral boundaries is not as drastic. Plate 2a, in fact, shows that the dayside maximum parallel velocity can occur at higher latitudes than the high-latitude auroral boundary. The comparison of O^+ parallel velocities with UVI auroral images demonstrates that the auroras are the sources of the observed upflowing ions. Also, in the absence of auroral processes, the bulk of the thermal O^+ falls earthward owing to lack of sufficient sustained upward acceleration in the dark polar cap regions. It should be noted that ionospheric upflows can also occur in the polar cap region. For example, *Peterson and Shelley* [1990] showed how theta auroras or polar cap auroras can cause energetic ion upflows within the nominal polar cap region.

In Plates 1 and 2a the parallel velocities decreased and turned downward from dayside to nightside across the isolated polar cap region. This trend is consistent with the CIF source for the O^+ distributions, as modeled by *Horwitz and Lockwood* [1985], in which the lower-energy O^+ ions demonstrated parabolic trajectories ending in the polar cap. Ions with higher cleft injection energies will reach higher altitudes and convect greater distances toward the nightside polar cap. The higher-energy ions could also attain greater downward velocities when reaching the satellite altitude, or they could escape. Therefore the result should be as measured with increasing magnitude of downward O^+ velocities from dayside to nightside across the isolated polar cap.

To further explore the CIF hypothesis, a 2 km s^{-1} downward traveling ion measured in the nightside polar cap at 78° on May 27, 1996, was traced back along a parabolic path to determine the feasibility of it having originated from the cleft. The particle was only considered to be acted upon by the gravitational potential and the $\mathbf{E} \times \mathbf{B}$ convective drift. The transit time was calculated to be 17.7 min for an O^+ ion to be ejected from 1000 km (on the dayside), up to 5690 km, and then back down to 5000 km with a final downward velocity of 2 km s^{-1}. Additional acceleration mechanisms during this transit as well as magnetic mirror forces were not considered, although these would certainly affect the transit time. The antisunward component of the convection velocity was found to be approximately 1.7 km s^{-1} during this period. Using this convection velocity mapped to 1000 km and the estimated transit time, it was found that the particle would travel antisunward approximately 30° in invariant latitude. Referring to Plate 2a, this estimated antisunward distance correlates very well with the location of the dayside aurora at 68° and 74°. Similarly, a 1 km s^{-1} upward traveling O^+ ion at 86° on the dayside of the polar cap was calculated to have a 11° antisunward convective distance during its 6.3 min transit time from 1000–5000 km. This again correlates very well with the location of the dayside aurora. Of course, further detailed modeling of the ion transport would be very useful in quantifying such comparisons with the data, which has been initiated by *Tu et al.*, [2000].

In Figures 1, 2, and 3 the O^+ densities decreased within the polar cap region from dayside to nightside. This relationship supports the observations made by *Su et al.*, [1998b]. Figures 1, 2, and 3 showed a strong increase in density slightly poleward of the point of maximum parallel velocity. This trend also supports the CIF model as being the source for ionospheric ions within the polar cap. Finally, the densities in Figures 2 and 3 show slight increases at the high-latitude nightside auroral boundary, as might be expected from additional auroral ionization there.

The CIF model [*Horwitz and Lockwood*, 1985] also suggested possible "hopping" trajectories for O^+ ions with large initial pitch angles. The quasiperiodic velocity variations in the polar cap region of Plate 2b may conceivably be due to a portion of the velocity distribution experiencing such "hopping" trajectories. The parallel velocities within the

dayside cleft region are relatively low for this pass, as is the relative auroral intensity (Figure 3). This may indicate that a substantial portion of the velocity distribution has large pitch angles in this region, therefore strengthening the possibility of hopping-type trajectories.

Acknowledgments. This research was supported in part by NASA grant NCC8-65 and NSF grant ATM-9612573 to the University of Alabama in Huntsville. Part of the support for B. A. Stevenson came from the Alabama Space Grant Consortium, through NASA training grant NGT5-40018. Support for T. E. Moore was through the NASA Global Geospace Science Program at Goddard Space Flight Center under UPN 370-17-43, while support for P. D. Craven was through the NASA Office of Space Flight at Marshall Space Flight Center under UPN 417-13-18. Support for G. Germany was through the NASA Global Geospace Science Program under subcontract 832213 to the University of Washington.

Janet G. Luhmann thanks William K. Peterson and Andrew W. Yau for their assistance in evaluating this paper.

References

Abe, T., B. A. Whalen, A. W. Yau, R. E. Horita, S. Watanabe, and E. Sagawa, EXOS-D (Akebono) SMS observations of the polar wind, *J. Geophys. Res.*, *98*, 11,191, 1993.

Abe, T., A. W. Yau, S. Watanabe, and E. Sagawa, On the ion acceleration in the polar wind (abstract), *Eos Trans. AGU*, *79(45)*, Fall Meet. Suppl., F758, 1998.

André, M., and A. W. Yau, Theories and observations of ion energization and outflow in the high latitude magnetosphere, *Space Sci. Rev.*, *80*, 27, 1997.

André, M., G. B. Crew, W. K. Peterson, A. M. Persoon, C. J. Pollock, and M. J. Engebretson, Ion heating by broadband low-frequency waves in the cusp/cleft, *J. Geophys. Res.*, *95*, 20,809, 1990.

Banks, P. M., and T. E. Holzer, The polar wind, *J. Geophys. Res.*, *73*, 6846, 1968.

Chandler, M. O., Observations of downward moving O^+ in the polar topside ionosphere, *J. Geophys. Res.*, *100*, 5795, 1995.

Chandler, M. O., J. H. Waite Jr., and T. E. Moore, Observations of polar ion outflows, *J. Geophys. Res.*, *96*, 1421, 1991.

Chang, T., G. B. Crew, H. Hershkowitz, J. R. Jasperse, J. M. Retterer, and J. D. Winningham, Transverse acceleration of oxygen ions by electromagnetic ion cyclotron resonance with broadband left-hand polarized waves, *Geophys. Res. Lett.*, *13*, 636, 1986.

Chappell, C. R., T. E. Moore, and J. H. Waite Jr., The ionosphere as a fully adequate source of plasma for the Earth's magnetosphere, *J. Geophys. Res.*, *92*, 5896, 1987.

Crew, G. B., T. Chang, J. M. Retterer, W. K. Peterson, D. A. Gurnett, and R. L. Huff, Ion cyclotron resonance heated conics: Theory and observations, *J. Geophys. Res.*, *95*, 3959, 1990.

Estep, G. M., Y.-J. Su, J. L. Horwitz, P. G. Richards, G. R. Wilson, and D. G. Brown, A dynamic coupled fluid-semikinetic model for ionosphere-magnetosphere plasma transport: Effects of ionization by soft electron precipitation (abstract), *Eos Trans. AGU*, *79*(17), Spring Meet. Suppl., S317, 1998.

Ganguli, S. B., The polar wind, *Rev. Geophys.*, *34*, 311, 1996.

Hirahara, M., J. L. Horwitz, T. E. Moore, G. A. Germany, and J. F. Spann, Relationship of topside ionospheric ion outflows to auroral forms and precipitation, plasma waves, and convection observed by Polar, *J. Geophys. Res.*, *103*, 17,391, 1998.

Horwitz, J. L., The ionosphere as a source for magnetospheric ions, *Rev. Geophys.*, *20*, 929, 1982.

Horwitz, J. L., Core plasma in the magnetosphere, *Rev. Geophys.*, *25*, 579, 1987.

Horwitz, J. L., The ionosphere's wild ride in outer space, *Rev. Geophys.*, *33*, 703, 1995.

Horwitz, J. L., and M. Lockwood, The cleft ion fountain: A two-dimensional kinetic model, *J. Geophys. Res.*, *90*, 9749, 1985.

Horwitz, J. L., and T. E. Moore, Four contemporary issues concerning ionospheric plasma flow to the magnetosphere, *Space Sci. Rev.*, *80*, 49, 1997.

Hultqvist, B., On the acceleration of positive ions by high-latitude, large-amplitude electric field fluctuations, *J. Geophys. Res.*, *101*, 27,111, 1996.

Hultqvist, B., R. Lundin, K. Stasiewicz, L. Block, P.-A. Lindqvist, G. Gustafsson, H. Koskinen, A. Bahnsen, T. A. Potemra, and L. J. Zanetti, Simultaneous observation of upward moving field-aligned energetic electrons and ions on auroral zone field lines, *J. Geophys. Res.*, *93*, 9765, 1988.

Knudsen, D. J., J. H. Clemmons, and J. E. Wahlund, Correlation between core ion energization, suprathermal electron bursts, and broadband ELF plasma waves, *J. Geophys. Res.*, *103*, 4171, 1998.

Lockwood, M., J. H. Waite Jr., T. E. Moore, J. F. E. Johnson, and C. R. Chappell, A new source of suprathermal O^+ ions near the dayside polar cap boundary, *J. Geophys. Res.*, *90*, 4099, 1985a.

Lockwood, M., M. O. Chandler, J. L. Horwitz, J. H. Waite Jr., T. E. Moore, and C. R. Chappell, The cleft ion fountain, *J. Geophys. Res.*, *90*, 9736, 1985b.

Miyake, W., T. Mukai, and N. Kaya, On the evolution of ion conics along the field line from EXOS-D observations, *J. Geophys. Res.*, *98*, 11,127, 1993.

Miyake, W., T. Mukai, and N. Kaya, On the origins of the upward shift of elevated (bimodal) ion conics in velocity space, *J. Geophys. Res.*, *101*, 26,961, 1996.

Moore, T. E., and D. C. Delcourt, The geopause, *Rev. Geophys.*, *33*, 175, 1995.

Moore, T. E., C. J. Pollock, R. L. Arnoldy, and P. M. Kintner, Preferential O^+ heating in the topside ionosphere, *Geophys. Res. Lett.*, *13*, 901, 1986.

Moore, T. E., et al., The thermal ion dynamics experiment and plasma source instrument, *Space Sci. Rev.*, *71*, 409, 1995.

Nagai, T., J. H. Waite Jr., J. L. Green, C. R. Chappell, R. C. Olsen, and R. H. Comfort, First measurements of supersonic polar wind in the polar magnetosphere, *Geophys. Res. Lett.*, *11*, 669, 1984.

Norvquist, P., M. Andre, and M. Tyrland, A statistical study of ion energization mechanisms in the auroral region, *J. Geophys. Res.*, *103*, 23,459, 1998.

Peterson, W. K., and E. G. Shelley, Origin of the plasma in a cross-polar cap auroral feature (theta aurora), *J. Geophys. Res.*, *95*, 18,969, 1990.

Pollock, C. J., M. O. Chandler, T. E. Moore, J. H. Waite Jr., C. R. Chappell, and D. A. Gurnett, A survey of upwelling ion event characteristics, *J. Geophys. Res.*, *95*, 18,969, 1990.

Schunk, R. W., and J. J. Sojka, Global ionosphere-polar wind system during changing magnetic activity, *J. Geophys. Res.*, *102*, 11,625, 1997.

Shelley, E. G., The auroral acceleration region: The world of beams, conics, cavitons, and other plasma exotica, *U.S. Natl. Rep. Int. Union Geod. Geophys. 1991–1994*, *Rev. Geophys.*, *33*, 709, 1995.

Shelley, E. G., W. K. Peterson, A. G. Ghielmetti, and J. Geiss, The polar ionosphere as a source of energetic magnetospheric plasma, *Geophys. Res. Lett.*, *9*, 941, 1982.

Su, Y.-J., J. L. Horwitz, G. R. Wilson, P. G. Richards, D. G. Brown, and C. W. Ho, Self-consistent simulation of the photoelectron-driven polar wind from 120 km to 9 R_E altitude, *J. Geophys. Res.*, *103*, 2279, 1998a.

Su, Y.-J., J. L. Horwitz, T. E. Moore, B. L. Giles, M. O. Chandler, P. D. Craven, M. Hirahara, and C. J. Pollock, Polar wind survey with the Thermal Ion Dynamics

Experiment/Plasma Source Instrument suite aboard Polar, *J. Geophys. Res., 103*, 29-305, 1998b.

Torr, M. R., et al., A far ultraviolet imager for the International Solar-Terrestrial Physics Mission, *Space Sci. Rev., 71*, 329, 1995.

Tu, J., X. Wu, J. L. Horwitz, B. A. Stevenson, T. E. Moore, and V. Coffey, DyFK simulation of field-aligned ion flows observed by Polar within convecting flux tubes over the polar ionosphere (abstract), *Eos Trans. AGU, 81*(48), Fall Meet. Suppl., SM22B–04, 2000.

Wilson, G. R., Semikinetic modeling of the outflow of ionospheric plasma through the topside collisional to collisionless transition region, *J. Geophys. Res., 97*, 10,551, 1992.

Wu, X.-Y., J. L. Horwitz, G. M. Estep, Y.-J. Su, D. G. Brown, and P. G. Richards, Dynamic fluid-kinetic (DyFK) modeling of auroral plasma outflow driven by soft electron precipitation and transverse ion heating, *J. Geophys. Res., 104*, 17,263, 1999.

Yau, A. W., and M. Andre, Sources of ion outflow in the high latitude ionosphere, *Space Sci. Rev., 80*, 1, 1997.

Yau, A. W., P. H. Beckwith, W.K. Peterson, and E. G. Shelley, Long-term (solar-cycle) and seasonal variations of upflowing ionospheric ion events at DE–1 altitudes, *J. Geophys. Res., 90*, 6395, 1985.

M. O. Chandler and P. D. Craven, Space Sciences Laboratory, Marshall Space Flight Center, MSFC, AL 35812

G. Germany and J. L. Horwitz, Center for Space Plasma and Aeronomic Research, University of Alabama in Huntsville, Huntsville, AL 35899

B. L. Giles and T. E. Moore, Laboratory for Extraterrestrial Physics, Goddard Space Flight Center, Greenbelt, MD 20771

G. K. Parks, Geophysics Program, University of Washington, Seattle, WA 98195–1650

B. A. Stevenson, Axcelis Technologies, Inc., 108 Cherry Hill Drive, Beverly, MA 01915 (adam.Stevenson@axcelis.com)

Y. J. Su, Space and Atmospheric Sciences, Los Alamos National Laboratory, Los Alamos, NM 87545

(Received June 20, 2000; revised April 2, 2001;
accepted April 2, 2001.)